STUDY ON RIGID-LIQUID COUPLING DYNAMICS OF THE SPACECRAFT WITH ARBITRARY AXISYMMETRICAL TANKS

Y. L. Yan **B. Z. Yue***

Department of Mechanics
School of Aerospace Engineering
Beijing Institute of Technology
Beijing, China

ABSTRACT

This article focus on the rigid-liquid coupling dynamics of the spacecraft with arbitrary axisymmetrical tanks with curved walls and top. The carrier velocity potential function was obtained according to the motion equations of a representative point in the tank of spacecraft, and the relative velocity potential function can be expressed as Gauss hypergeometric series. The Hamilton's variational principle was applied to derive the governing equations of liquid sloshing based on the profile of hydrostatic shape of free liquid surface. The dynamic equations of modal coordinates were established through the Galerkin method. The state equations of coupled motion of main rigid platform of the spacecraft were deduced by using the Lagrange's equations in term of general quasi-coordinates. Thruster firing was actuated to the coupled system to analyze the rigid-liquid coupled dynamic behaviors. Computer numerical simulations was carried out to confirm the validity of the method developed in this paper.

Keywords: Axisymmetrical tank, Low-gravity, Rigid-liquid coupling system, Liquid-filled spacecraft.

1. INTRODUCTION

The advanced spacecraft always contains a large amount of liquid propellant to execute complex space missions such as trajectory and attitude adjustments, maneuvers, rendezvous and docking. The rigid body motions and liquid propellant sloshing constitute the rigid-liquid coupled spacecraft systems, and complicated dynamical behaviors will be occurred in the coupled system [1, 2]. If the rigid-liquid coupled spacecraft system model is not constructed accurately, the efficiency and accuracy of the spacecraft controlling system will be significantly decreased [3, 4], which will result in the failure of the spacecraft missions and unfavorable results. It should be noted that the liquid surface tension will play a significant role in the low-gravity environment. The stationary liquid surface will be seriously curved due to capillary effect [5]. The sloshing natural frequency will be reduced in low-gravity, which induces low-frequency vibration and instability of the spacecraft. Thus, liquid sloshing analysis in low-gravity is more complicated than it is in normal gravity, especially for an arbitrary axisymmetrical tank.

Axisymmetrical tanks are widely used in the aerospace engineering. Generally, the sloshing behaviors for rectangle tanks [6, 7] and cylinder tanks [8-11] were solved by analytic methods, while seldom analytic researches focus on the sloshing problem in arbitrary axisymmertical tanks with curved wall and top, such as spherical tank, prolate spherical tank, oblate spherical tank, Cassini tank. One reason is that there are no proper characteristic functions to describe the liquid sloshing in arbitrary axisymmertical tanks. McIver [12] used special coordinate system to solve this problem and obtained the frequencies of free oscillations of the fluid in spherical tanks in normal gravity. Utsumi studied the low-gravity liquid sloshing with spherical coordinate system and expressed velocity potential function in term of the Gauss hypergeometric functions. The response of liquid sloshing in a spherical tank was considered for the case of lateral [13] and axial excitations [14]. The equivalent sloshing model [15], sloshing parameters [16] and liquid damping [17] of the arbitrary axisymmertical tanks were also researched. The coupled nonlinear dynamic system of a liquid-filled spherical tank which can be excited discretionarily was studied analytically [18]. Natural sloshing modes of a spherical tank shape were also discussed analytically [19]. In addition, the equivalent mechanical model, numerical and experimental methods are also useful approaches to discuss rigid-liquid coupled effect of the liquid-filled spacecraft system. The main dynamical effect of lateral sloshing can be expressed by an equivalent mechanical model, such as spring-mass model and spherical pendulum

* Corresponding author (bzyue@bit.edu.cn)

DOI : 10.1017/jmech.2018.15
Copyright © 2018 The Society of Theoretical and Applied Mechanics
https://doi.org/10.1017/jmech.2018.15 Published online by Cambridge University Press

model [20-22]. Although the equivalent mechanical model was known to work with a wide range of tank geometries and liquid properties, it cannot reflect the complex rigid-liquid coupled nonlinear dynamic behaviors. Dodge *et al*. [23] analyzed the small amplitude low-gravity sloshing in axisymmetric tanks with computational fluid dynamics (CFD). The influence of liquid sloshing on the dynamics of spacecraft was studied [24] with the theoretical approach and CFD, and the related results were compared to the experimental data of Sloshsat FLEVO. The research conclusions show that the liquid sloshing will decrease the stability of spacecraft. The fundamental sloshing mode of a liquid in an axisymmetric tank was studied by using finite-element method [25], and the complicated three-dimensional numerical computations was reduced to the two-dimensional profile. The CFD is an effective method to deal with sloshing liquid in containers. The computational expense will grow dramatically as the complexity of the problem increases.

In previous studies, the response and sloshing parameters of an arbitrary axisymmertical tank were ascertained by analytical methods, which mainly focused on liquid behaviors in the tanks. Furthermore, little analytic analysis has been done on the rigid-liquid coupling effect of the liquid-filled spacecraft with an arbitrary axisymmertical tank. In order to solve this problem, this paper investigate the rigid-liquid coupled dynamics of the spacecraft with the arbitrary axisymmertical tank by using the velocity potential function. The expression of the carrier velocity potential function was calculated by analyzing a representative point in the tank of spacecraft, and the relative velocity potential function was determined analytically in terms of Gauss hypergeometric series. The dynamic equations of modal coordinates are developed through the Galerkin method. The governing equations of main rigid platform of the spacecraft are derived by using the Lagrange's equations in term of general quasi-coordinates. The external disturbance and thruster firing are applied to the rigid-liquid coupled system to analyze the coupling effect between spacecraft motion and liquid sloshing. Compared to other approaches such as CFD and the equivalent mechanical model, this method is able to benefit from higher efficiency and accuracy, lower calculation and memory consumption.

2. MATHEMATIC MODEL OF COUPLED SYSTEM

The mathematic model and dynamical equations of the rigid-liquid coupled spacecraft system will be derived in this section. For convenience, we make these assumptions: (1) The fuel tank is a rigid container, (2) the liquid fuel motion is incompressible, nonviscous, and nonrotational, (3) the oscillatory displacement of the liquid fuel surface is small enough to be expressed within the framework of the linear theory. These assumptions allow classical potential flow theory to be used.

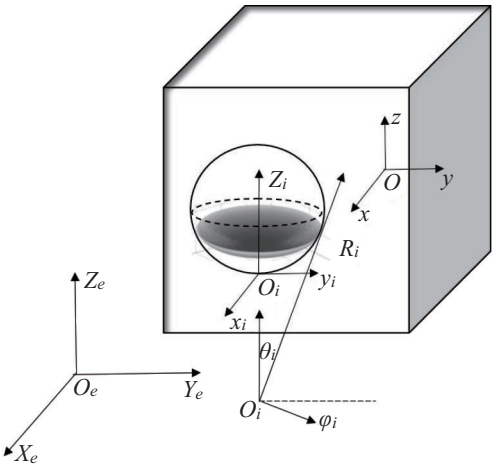


Fig. 1 A schematic representation of the rigid-liquid coupled spacecraft system.

2.1 Coordinate System of Spacecraft

A schematic representation of the rigid-liquid coupled spacecraft system is illustrated in Fig. 1. The rigid container, which is fixed on the main rigid platform of the spacecraft, has structural frequencies spectrally separated from dominant propellant sloshing modes. The orthogonal coordinates systems $O_eX_eY_eZ_e$ and $Oxyz$ are the inertial reference frame and the body-fixed reference frame, respectively. The point O is the mass center of the spacecraft. The axes Ox, Oy, Oz are the principal axes of the rigid spacecraft. Axis Oz points toward the mass center of the Earth. Suppose that $\boldsymbol{\theta} = [\theta_x, \theta_y, \theta_z]^T$ is the attitude vector of the main rigid platform relative to the frame $O_eX_eY_eZ_e$, and $\boldsymbol{r}_{O_eO}$ is the position vector of the main rigid platform relative to the frame $O_eX_eY_eZ_e$. The coordinate transform matrix between the frame $O_eX_eY_eZ_e$ and the frame $Oxyz$ is:

$$\boldsymbol{C} = \begin{bmatrix} c_y c_z & c_x s_z + s_x s_y c_z & s_x s_z - c_x s_y c_z \\ -c_y s_z & c_x c_z - s_x s_y s_z & s_x c_z + c_x s_y s_z \\ s_y & -s_x c_y & c_x c_y \end{bmatrix} \tag{1}$$

where $s_k = \sin\theta_k$, $c_k = \cos\theta_k$, $k = x, y, z$ (the same below).

Suppose $\boldsymbol{v}_O = [v_x, v_y, v_z]^T$ is the translational velocity relative to the frame $O_eX_eY_eZ_e$, $\boldsymbol{\omega} = [\omega_x, \omega_y, \omega_z]^T$ is the angular velocity of the frame $Oxyz$ with respect to the frame $O_eX_eY_eZ_e$. The following transformations can be obtained.

$$\boldsymbol{v}_O = \boldsymbol{C}\dot{\boldsymbol{r}}_{O_eO}, \quad \boldsymbol{\omega} = \boldsymbol{D}\dot{\boldsymbol{\theta}} \tag{2}$$

where $\boldsymbol{D}$ is dependent on the attitude vector $\boldsymbol{\theta}$, the formulation of $\boldsymbol{D}$ is as follows.

$$\boldsymbol{D} = \begin{bmatrix} c_y c_z & s_z & 0 \\ -c_y s_z & c_z & 0 \\ s_y & 0 & 1 \end{bmatrix} \tag{3}$$

The orthogonal coordinates system $o_ix_iy_iz_i$ is located at

https://doi.org/10.1017/jmech.2018.15 Published online by Cambridge University Press

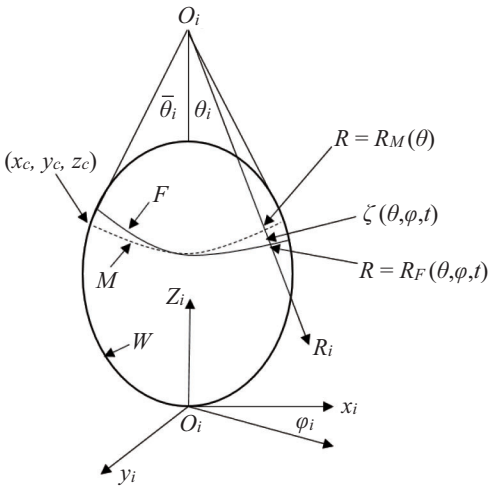


Fig. 2 A schematic representation of an arbitrary axisymmetric tanks.

the nadir of the axisymmetric tanks in the ith tank, which is called the tank-fixed reference frame. The coordinate transform matrix between the frame $o_ix_iy_iz_i$ and the frame $Oxyz$ is $\boldsymbol{C}_1$. $\boldsymbol{C}_1$ is related to the tank shape and installation orientation. The matrix $\boldsymbol{C}_1$ can be chosen as the unit matrix if the tank is spherical tank or the symmetry axis of the tank o_iz_i is in parallel with axis Oz. In order to simplify the derivations, the $\boldsymbol{C}_1$ will be set as unit matrix in the following section. Owing to surface tension effect, the stationary liquid surface will be curved seriously. The spherical coordinate system $O_iR_i\theta_i\varphi_i$ is established to research the liquid sloshing in the tank, where $\theta_i \in [0, \bar{\theta}_i]$, $\varphi_i \in [0, 2\pi]$, as depicted in Fig. 2. The origin O_i is chosen as the apex of the cone whose side wall is tangent to the container wall at the contact line of the stationary liquid interface. The liquid surface displacement ζ is considered in R_i direction. The orthogonal coordinate of O_i is (0, 0, h_i) in the frame $o_ix_iy_iz_i$. The stationary and disturb liquid surfaces can be represented by M and F, as the dashed line and solid line shown in Fig. 2, respectively. The tank wall is denoted by W. The profile of M can be calculated though the governing differential equation of the stationary liquid surface based on Young-Laplace equations [5]. In terms of the spherical coordinates, the stationary surface, tank wall, the disturb liquid surfaces can be expressed as

$$M: R = R_M(\theta),$$
$$F: R = R_F(\theta,\varphi,t) = R_M(\theta) + \zeta(\theta,\varphi,t),$$
$$W: R = R_W(\theta).$$

Intersection of the stationary liquid surface and the tank wall is called contact line, the orthogonal coordinate of an arbitrary point in the contact line can be denoted by (x_c, y_c, z_c). Due to the symmetrical characteristic of the tank, the value of z_c is independent of the chosen of the point in contact line. The half-height of the container in vertical direction is R_0. The origin O_i of the frame $O_iR_i\theta_i\varphi_i$ will be above the tank for $z_c > R_0$ or below the tank for $z_c < R_0$. In order to describe both situations, the parameter ε will be introduced: $\varepsilon = \begin{cases} 1 & z_c > R_0 \\ -1 & z_c < R_0 \end{cases}$.

The vector of a representative point p in the tank of spacecraft is $\boldsymbol{r}_{o_ip}$ relative to the frame $o_ix_iy_iz_i$, which can be expressed as (x_{pi}, y_{pi}, z_{pi}) and (R_{pi}, θ_{pi}, φ_{pi}) in the frames $o_ix_iy_iz_i$ and $O_iR_i\theta_i\varphi_i$, respectively. The transformation of two coordinates is:

$$x_{pi} = R_{pi}\sin\theta_{pi}\cos\varphi_{pi},$$
$$y_{pi} = R_{pi}\sin\theta_{pi}\sin\varphi_{pi},$$
$$z_{pi} = h_i - \varepsilon R_{pi}\cos\theta_{pi}$$

Denoting the position of the origin o_i of the frame $o_ix_iy_iz_i$ by vector $\boldsymbol{r}_{Oo_i} = [x_i, y_i, z_i]^T$, and the position of p relative to the frame $O_eX_eY_eZ_e$ by $\boldsymbol{r}_{O_ep}$, which can be expressed as:

$$\boldsymbol{r}_{O_ep} = \boldsymbol{r}_{O_eO} + \boldsymbol{C}^T\boldsymbol{r}_{Op} = \boldsymbol{r}_{O_eO} + \boldsymbol{C}^T(\boldsymbol{r}_{Oo_i} + \boldsymbol{r}_{o_ip}) \tag{4}$$

Then, the velocity vector of p relative to the frame $O_eX_eY_eZ_e$ is

$$\boldsymbol{v}_{pi} = \boldsymbol{v}_O + \boldsymbol{\omega}\times(\boldsymbol{r}_{Oo_i} + \boldsymbol{r}_{o_ip}) \tag{5}$$

2.2 The Derivation of Velocity Potential

According to the principle of superposition, it is possible to divide the total velocity potential function ϕ of liquid sloshing into a relative potential function ϕ_r and a carrier potential function ϕ_e [26]. The potential function ϕ_e is obtained basing on Eq. (5), which can be represented in the spherical coordinate.

$$\phi_e = (v_x + \omega_y z_i - \omega_z y_i)R_i\sin\theta_i\cos\varphi_i + (v_y + \omega_z x_i - \omega_x z_i)R_i\sin\theta_i\sin\varphi_i + (v_z + \omega_x y_i - \omega_y x_i)(h_i - \varepsilon R_i\cos\theta_i) \tag{6}$$

The expression of relative potential function ϕ_r will be considered in the following parts. For the liquid sloshing in the tank, the variational principle can be written as

$$\delta\int_{t_1}^{t_2}\left[\iiint_V(p_l - p_g)\mathrm{d}V - \iint_F\sigma\mathrm{d}F - \iint_{W_1}\sigma_1\mathrm{d}W_1 - \iint_{W_2}\sigma_2\mathrm{d}W_2\right]\mathrm{d}t = 0 \tag{7}$$

where p_l is the liquid pressure; p_g is the gas pressure; σ, σ_1, σ_2 are the surface energy per unit area associated with the liquid-gas interface F, liquid-solid interface W_1, solid-gas interface W_2. The liquid pressure of the liquid-gas interface

https://doi.org/10.1017/jmech.2018.15 Published online by Cambridge University Press

p_l could be split into static liquid pressure $p_{l,st}$ and dynamic liquid pressure $p_{l,dy}$

$$p_{l,st} = p_0 - \varepsilon\rho_f g[R_M(0) - R_M(\theta)\cos\theta], \quad p_{l,dy} = -\rho_f\left[\frac{\partial\phi_r}{\partial t} + \frac{1}{2}(\nabla\phi_r)^2\right]$$

where p_0 is static liquid pressure at the intersection of the vertical symmetry axis and the stationary liquid-gas interface; ρ_f is liquid density; g is effective gravitational acceleration. Submit the related expressions into Eq. (7), the governing equations of the liquid sloshing could be obtained.

$$\begin{aligned}
&\rho_f\varepsilon\int_0^{2\pi}\int_0^{\bar\theta}\int_{R_M}^{R_W}\nabla^2\phi_r\delta\phi_r R^2\sin\theta\mathrm{d}r\mathrm{d}\theta\mathrm{d}\varphi - \rho_f\varepsilon\int_0^{2\pi}\int_0^{\bar\theta}\left(\left.\frac{\partial\phi_r}{\partial R}\right|_{R=R_W} - \frac{R_{W\theta}}{R_W^2}\left.\frac{\partial\phi_r}{\partial\theta}\right|_{R=R_W}\right)\delta\phi_r|_{R=R_W}\\
&\times R_W^2\sin\theta\mathrm{d}\theta\mathrm{d}\varphi - \rho_f\varepsilon\int_0^{2\pi}\int_0^{\bar\theta}\left(\frac{\partial\zeta}{\partial t} - \left.\frac{\partial\phi_r}{\partial R}\right|_{R=R_M} + \frac{R_{M\theta}}{R_M^2}\left.\frac{\partial\phi_r}{\partial\theta}\right|_{R=R_M}\right)\delta\phi_r|_{R=R_M} R_M^2\sin\theta\mathrm{d}\theta\mathrm{d}\varphi\\
&+\int_0^{2\pi}\int_0^{\bar\theta}\left\{\varepsilon(p_g - p_0) + \rho_f g(R_M(0) - R_M(\theta)\cos\theta) + \varepsilon\rho_f\left.\frac{\partial\phi_r}{\partial t}\right|_{R=R_M}\right.\\
&+\varepsilon\rho_f R_M\sin\theta[\cos\varphi\times(\dot v_x + \dot\omega_y z_i - \dot\omega_z y_i) + (\dot v_y + \dot\omega_z x_i - \dot\omega_x z_i)\sin\varphi]\\
&+\varepsilon\rho_f(h_i - \varepsilon R_M\cos\theta)(\dot v_z + \dot\omega_x y_i - \dot\omega_y x_i) - \rho_f[g + (\dot v_z + \dot\omega_x y_i - \dot\omega_y x_i)]\zeta\cos\theta\\
&-\sigma(S_{0M} + S_{1M}\zeta + S_{2M}\zeta_\theta + S_{3M}\zeta_{\theta\theta} + S_{4M}\zeta_{\varphi\varphi})\}\times R_M^2\delta\zeta\sin\theta\mathrm{d}\theta\mathrm{d}\varphi\\
&+\varepsilon\sigma\int_0^{2\pi}(R_M^2 + R_{M\theta}^2)^{-3/2}(R_M\zeta_\theta - R_{M\theta}\zeta)\delta\zeta|_{R=R_M} R_M^2\sin\bar\theta\mathrm{d}\varphi = 0
\end{aligned} \tag{8}$$

Equation (8) contains the condition of continuity in the liquid domain, the compatibility condition for the liquid surface displacement at the tank wall, the kinematic and dynamic conditions in the gas-liquid interface and the contact angle condition. Detailed descriptions of the symbols in Eq. (8) are shown in Appendix.

In the spherical coordinate, the Laplace equation becomes

$$\nabla^2\phi_r = \frac{\partial^2\phi_r}{\partial R^2} + \frac{2}{R}\frac{\partial\phi_r}{\partial R} + \frac{1}{R^2}\frac{\partial^2\phi_r}{\partial\theta^2} + \frac{\cot\theta}{R^2}\frac{\partial\phi_r}{\partial\theta} + \frac{1}{R^2\sin^2\theta}\frac{\partial^2\phi_r}{\partial\varphi^2} = 0$$

Since integrating range of θ is $0 \le \theta \le \bar\theta$ and $\bar\theta < \pi/2$, the orthogonality cannot be ensured through the associated Legendre functions. By introducing the Gauss hypergeometric series, the relative velocity potential function and surface displacement can be expressed as

$$\begin{aligned}
\phi_r(R,\theta,\varphi,t) &= \sum_{m=0}^{\infty}\sum_{k=1}^{\infty}\left[a_{mk}\left(R/l_a\right)^{-(1+\alpha_{mk})} + b_{mk}\left(R/l_b\right)^{\alpha_{mk}}\right]\Theta_{mk}(\cos m\varphi\dot q_m + \sin m\varphi\dot p_m)\\
\zeta(\theta,\varphi,t) &= \sum_{m=0}^{\infty}\sum_{k=1}^{\infty}c_{mk}\Theta_{mk}(\cos m\varphi q_m + \sin m\varphi p_m)
\end{aligned} \tag{9}$$

where q_m, p_m, m = 0,1,2,… are the modal coordinates; a_{mk}, b_{mk}, c_{mk} are arbitrary real constants, which are related to the natural frequency [13]. By omitting the excitation term, the natural frequencies of the liquid sloshing can be computed with the Galerkin method. c_{mk} is the eigenvector, which yields the m th eigenmode of liquid surface displacement. a_{mk}, b_{mk} are determined by c_{mk}. l_a, l_b are the minimum and maximum of R, which are used to improve the convergence speed of the series. i.e.

$$\begin{cases} l_a = R_M, l_b = R_W & \varepsilon = 1\\ l_a = R_W, l_b = R_M & \varepsilon = -1 \end{cases}$$

The formulation of characteritic function $\Theta_{mk}(\theta)$ is

$$\Theta_{mk}(\theta) = \sin^m\theta F(m - \alpha_{mk}, \alpha_{mk} + m + 1, m + 1, (1 - \cos\theta)/2)$$

where $F(\alpha,\beta,\gamma,x)$ is the Gauss hypergeometric series, characteristic values α_{mk} can be obtained by solving dynamical contact line conditions $\dfrac{d\Theta_{mk}(\bar\theta)}{d\theta} = 0$. The total liquid sloshing velocity potential function can be drawn from Eq. (6)

https://doi.org/10.1017/jmech.2018.15 Published online by Cambridge University Press

and Eq. (9), i.e.

$$\phi=\sum_{m=0}^{\infty}\sum_{k=1}^{\infty}\left[a_{mk}\left(R/l_a\right)^{-(1+\alpha_{mk})}+b_{mk}\left(R/l_b\right)^{\alpha_{mk}}\right]\Theta_{mk}(\dot{q}_m\cos m\varphi+\dot{p}_m\sin m\varphi)$$
$$+[(v_x+\omega_y z_i-\omega_z y_i)\times R_i\sin\theta_i\cos\varphi_i+(v_y+\omega_z x_i-\omega_x z_i)R_i\sin\theta_i\sin\varphi_i+(v_z+\omega_x y_i-\omega_y x_i)(h_i-\varepsilon R_i\cos\theta_i)] \quad (10)$$

2.3 Governing Equations of the Coupled Spacecraft System

The liquid sloshing velocity potential function ϕ_e was related to the velocity and angular velocity of the spacecraft. Considering variations with the sloshing modal coordinates q_m, p_m, m = 0,1,2,… in Eq. (9), then

$$\delta\phi_r=\sum_{l=1}^{\infty}\left[a_{0l}\left(R/l_a\right)^{-(1+\alpha_{0l})}+b_{0l}\left(R/l_b\right)^{\alpha_{0l}}\right]\Theta_{0l}\delta\dot{q}_0$$
$$+\sum_{n=1}^{\infty}\sum_{l=1}^{\infty}\left[a_{nl}\left(R/l_a\right)^{-(1+\alpha_{nl})}+b_{nl}\left(R/l_b\right)^{\alpha_{nl}}\right]\Theta_{nl}(\delta\dot{q}_n\cos n\varphi+\delta\dot{p}_n\sin n\varphi)$$
$$\delta\zeta=\sum_{l=1}^{\infty}c_{0l}\Theta_{0l}\delta q_0+\sum_{n=1}^{\infty}\left(\sum_{l=1}^{\infty}c_{nl}\Theta_{nl}\delta q_n+\sum_{l=1}^{\infty}c_{nl}\Theta_{nl}\delta p_n\right) \quad (11)$$

Submit Eq. (11) into Eq. (8), due to the variations δq_m, δp_m, m = 0,1,2,… are arbitrary and independent of one another, the liquid sloshing equations could be derived

$$M_0\ddot{q}_0+K_0q_0=\beta_0,\quad M_1\ddot{q}_1+K_1q_1=\beta_1,\quad M_1\ddot{p}_1+K_1p_1=\beta_2,\quad M_m\ddot{q}_m+K_mq_m=0,\quad M_m\ddot{p}_m+K_mp_m=0. \quad (12)$$

where m = 2,3,…, the detailed descriptions of the symbols in Eq. (12) are shown in Appendix.

The sloshing force and moment are the critical sloshing parameters for the dynamical analysis for the rigid-liquid coupled spacecraft system. The sloshing forces $\boldsymbol{F}_i=[F_{xi},F_{yi},F_{zi}]^T$ and moments $\boldsymbol{M}_i=[M_{xi},M_{yi},M_{zi}]^T$ in the ith tank mainly include the liquid pressure acting on the tank wall, and the surface tension over the wetted surface of the tank wall and the contact line. For brevity, the component of $\boldsymbol{F}_i$, $\boldsymbol{M}_i$ along the x-direction will be given and the detailed descriptions of sloshing forces and sloshing moments can also be found in Appendix.

$$F_{xi}=\iint_W p_d(\boldsymbol{N}_W\cdot\boldsymbol{e}_x)\mathrm{d}W+\int_C(p_g-p_c)\zeta(\boldsymbol{N}_W\cdot\boldsymbol{e}_x)\mathrm{d}C+\sigma\int_C(\boldsymbol{t}_F\cdot\boldsymbol{e}_x)\mathrm{d}C,$$
$$M_{xi}=\iint_W p_d[(\boldsymbol{N}_W\cdot\boldsymbol{e}_z)y-(\boldsymbol{N}_W\cdot\boldsymbol{e}_y)z]\mathrm{d}W+\sigma\int_C[(\boldsymbol{t}_F\cdot\boldsymbol{e}_z)y-(\boldsymbol{t}_F\cdot\boldsymbol{e}_y)z]\mathrm{d}C$$
$$+\int_C(p_g-p_c)\zeta[(\boldsymbol{N}_W\cdot\boldsymbol{e}_z)y-(\boldsymbol{N}_W\cdot\boldsymbol{e}_y)z]\mathrm{d}C.$$

where $\boldsymbol{N}_F$ is the unit normal vector of F pointing into liquid domain; $\boldsymbol{N}_W$ is the unit normal vector of W pointing outwards from liquid domain; $\boldsymbol{t}_F$ is the unit vector both parallel to $\boldsymbol{N}_W$ and perpendicular to $\boldsymbol{N}_F$, i.e.

$$\boldsymbol{t}_F=\frac{\boldsymbol{N}_F\times(\boldsymbol{N}_F\times\boldsymbol{N}_W)}{|\boldsymbol{N}_F\times(\boldsymbol{N}_F\times\boldsymbol{N}_W)|}$$

As Eq. (2) shown, $\boldsymbol{v}_O$ and $\boldsymbol{\omega}$ are the velocity vector and angular vector of the main rigid platform in terms of components along $Oxyz$, respectively. Thus, the Lagrange's function of the main rigid platform of the spacecraft can be expressed as

$$L=\frac{1}{2}m_0\boldsymbol{v}_O^T\boldsymbol{v}_O+\frac{1}{2}\boldsymbol{\omega}^T\boldsymbol{J}_0\boldsymbol{\omega} \quad (13)$$

where m_0, $\boldsymbol{J}_0$ are the total mass and inertial matrix of the main rigid platform of the spacecraft, respectively. The Lagrange's equations in term of general quasi- coordinates were used to build the state equations of the coupled motion of main rigid platform of the spacecraft

$$\frac{\mathrm{d}}{\mathrm{d}t}\frac{\partial L}{\partial\boldsymbol{v}_O}+\boldsymbol{\omega}\times\frac{\partial L}{\partial\boldsymbol{v}_O}-\boldsymbol{C}\frac{\partial L}{\partial\boldsymbol{r}_{O_eO}}=\boldsymbol{F}_0+\sum_{i=1}^{N}\boldsymbol{F}_i$$
$$\frac{\mathrm{d}}{\mathrm{d}t}\frac{\partial L}{\partial\boldsymbol{\omega}}+\boldsymbol{\omega}\times\frac{\partial L}{\partial\boldsymbol{\omega}}+\boldsymbol{v}_O\times\frac{\partial L}{\partial\boldsymbol{v}_O}-\boldsymbol{D}^{-1}\frac{\partial L}{\partial\boldsymbol{\theta}}=\boldsymbol{M}_0+\sum_{i=1}^{N}(\boldsymbol{r}_{Oo_i}\times\boldsymbol{F}_i+\boldsymbol{M}_i) \quad (14)$$

where $\boldsymbol{F}_0$, $\boldsymbol{M}_0$ are the external nonconservative forces and moments, respectively. $\boldsymbol{F}_i$, $\boldsymbol{M}_i$ are the sloshing forces and

https://doi.org/10.1017/jmech.2018.15 Published online by Cambridge University Press

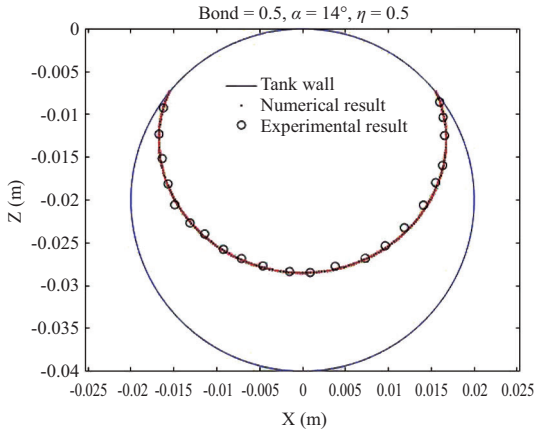


Fig. 3 The stationary liquid-vapor interface shape in the low gravity environment.

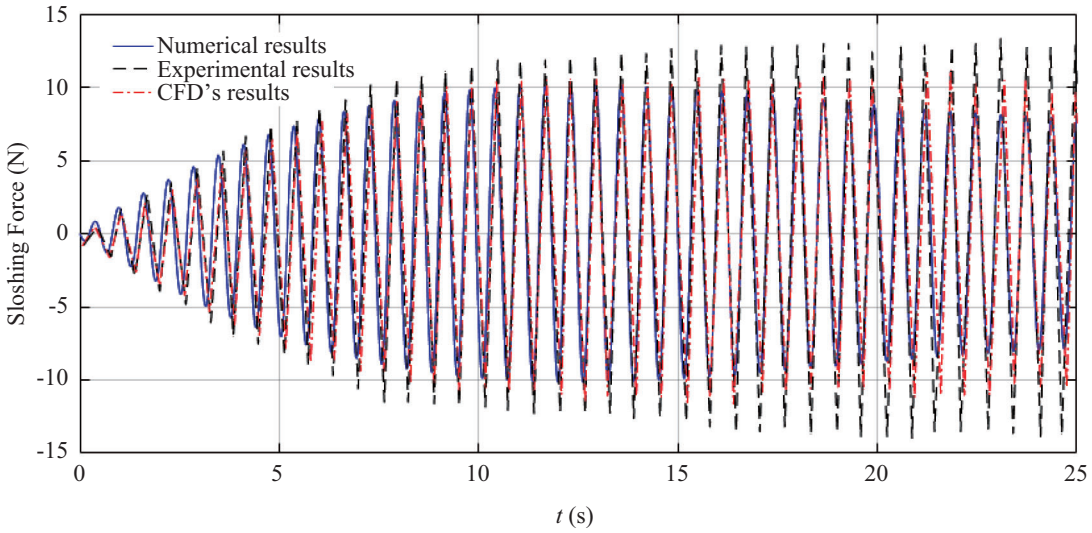


Fig. 4 The liquid sloshing force response of the spherical tank with the transverse excitation.

moments in the ith tank, respectively, N is the total number of tanks. Combined with the kinematic Eq. (2) and dynamic Eq. (14) equations of the main rigid platform of the spacecraft, and the governing equations Eq. (12) of the modal coordinates of sloshing velocity potential function, the state equations of the rigid-liquid coupled spacecraft were developed.

3. NUMERICAL SIMULATIONS AND DISCUSSIONS

In order to verify the mathematical model and analyze the coupling dynamics of the rigid-liquid coupled spacecraft system in the paper, the numerical simulations via computer will be considered in this section.

Example 1: The stationary liquid-vapor interface shape in the low gravity environment.

The shape of the liquid-vapor interface is the foundation of the liquid sloshing dynamical behaviors. The interface shape of the spherical tank by numerical methods will be compared to the experimental results [27]. The tank is spherical tank with radius of 0.02 m. The liquid density is $\rho_f = 998.2$ kg/m^3, interface tension of the liquid propellant is $\sigma = 0.0728$ N/m, Bond number is 0.5, contact angle α is 14 degrees, and liquid filled ratio η is 0.5. The interface shape is illustrated in Fig. 3. The blue solid line is the tank wall, the red dot line is the interface shape computed by numerical methods, and the black circles are the experimental results. The results verify the correctness of the numerical results of the interface shapes in this paper.

Example 2: The liquid sloshing force response of the spherical tank with the transverse excitation.

The sloshing force and moment are the important sloshing parameters in the research of rigid-liquid coupled dynamical behaviors. The sloshing force in the transverse excitation by numerical methods will be compared to the experimental and CFD results [28]. The tank is spherical tank with radius of 0.148 m, and the liquid filled ratio is 0.5. The experimental environment is normal gravity. The sloshing force response is shown in Fig. 4. The blue solid line is the numerical results in

https://doi.org/10.1017/jmech.2018.15 Published online by Cambridge University Press

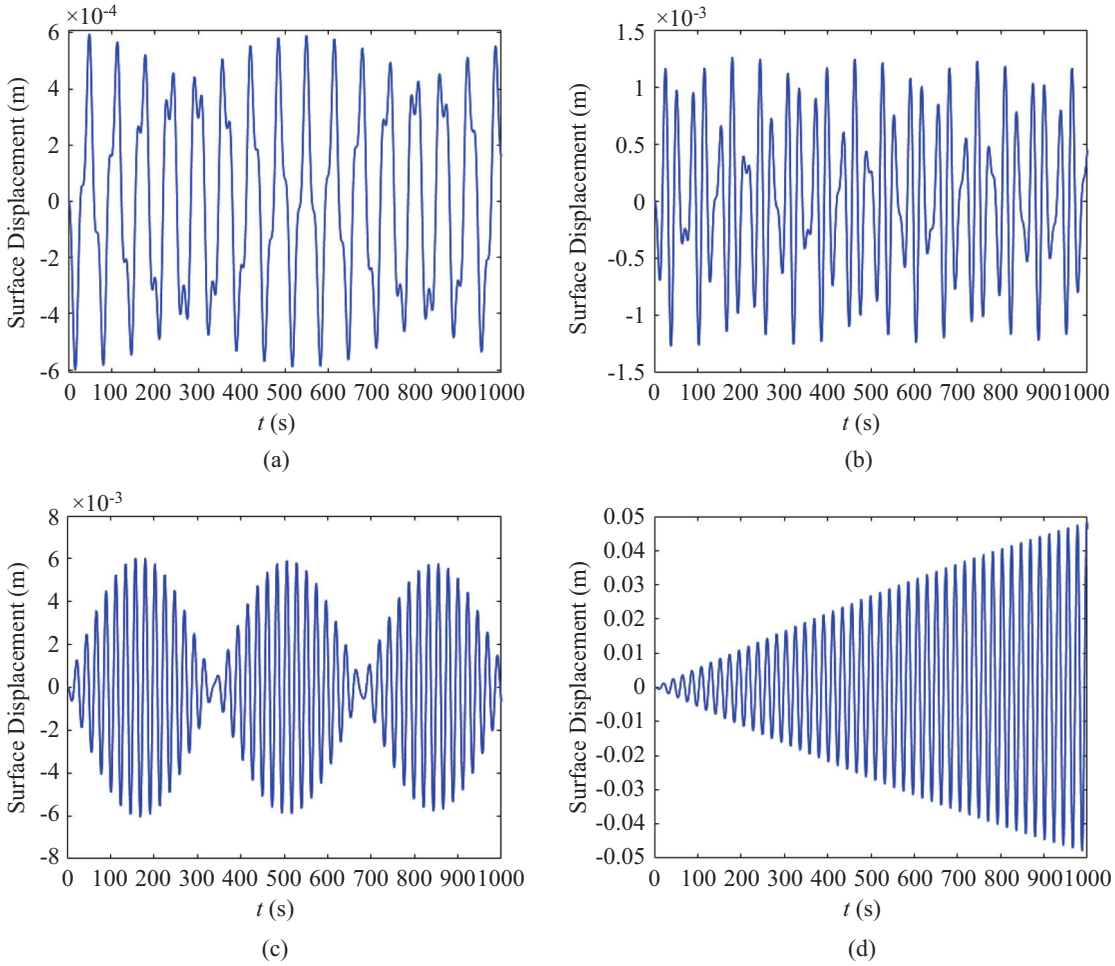


Fig. 5 Response of sloshing wave height at the tank wall with different external excitation frequency, (a) 0.1 rad/s, (b) 0.2 rad/s, (c) 0.27 rad/s, (d) 0.29 rad/s.

this paper, the black dot line is experimental results [28], and the red dash-dot line is the CFD's results. The numerical results in this paper agree well with experimental and CFD results [28].

In order to complete the numerical simulations, the governing equations Eq. (12) of the modal coordinates, and the kinematic Eq. (2) and dynamic Eq. (14) equations of the rigid platform are reduced order to generate ordinary differential equation system. Then, the equations are resolved by the classical fourth-order Runge-Kutta method. The response of sloshing parameters and rigid platform will be computed by numerical results. The response of the coupled rigid-liquid spacecraft system will be discussed by two examples. The parameters of the rigid-liquid coupled spacecraft system are as follows: the total mass of the main rigid platform of the spacecraft is m_0 = 800 kg inertial matrix of the main rigid platform is $\boldsymbol{J}_0$ = diag (1200,1200,1500) kg·m^2 i.e. Oz axis is the symmetry axis of the main rigid platform. The liquid tank is a spherical container with radius of R_0 = 0.4 m, and liquid filled ratio is 0.4. The liquid density is ρ_f = 1000 kg/m^3, interface tension of the liquid propellant is σ = 0.0725 N/m, effective gravity is g = 0.02 m/s^2.

Example 3: The influence of external harmonic excitation on the coupled system.

The response of the coupled spacecraft system under the harmonic disturbance excitation will be viewed. The disturbance moment can be expressed as $M_y = 0.1 \sin\omega_0 t$, where ω_0 is the frequency of external harmonic excitation. Assume that the center of the spherical tank is located on the origin of the frame $Oxyz$. To illustrate the dynamical behaviors under different excitation frequency, the external excitation frequency will be chosen as 0.1 rad/s, 0.2 rad/s, 0.27 rad/s, 0.29 rad/s.

The response of sloshing wave height at the tank wall is shown in Fig. 5. The liquid sloshing reveals different kinds of dynamical behaviors under different external excitation frequencies as shown in the simulation results, such as quasi-periodical motion (Fig. 5(a)), chaos (Fig. 5(b)), beat vibration (Fig. 5(c)), resonance (Fig. 5(d)). Although the external moment is small, the large amplitude of sloshing wave height will be produced at the tank wall for the last two situations, which contributes a non-negligible influence on attitude and position of the spacecraft vehicle.

Example 4: The influence of the zero-momentum step driver mode on the coupled system.

In order to realize the adjustment of the attitude and position of the spacecraft, the controllers of the spacecraft system using the momentum wheel or gas jet are

https://doi.org/10.1017/jmech.2018.15 Published online by Cambridge University Press

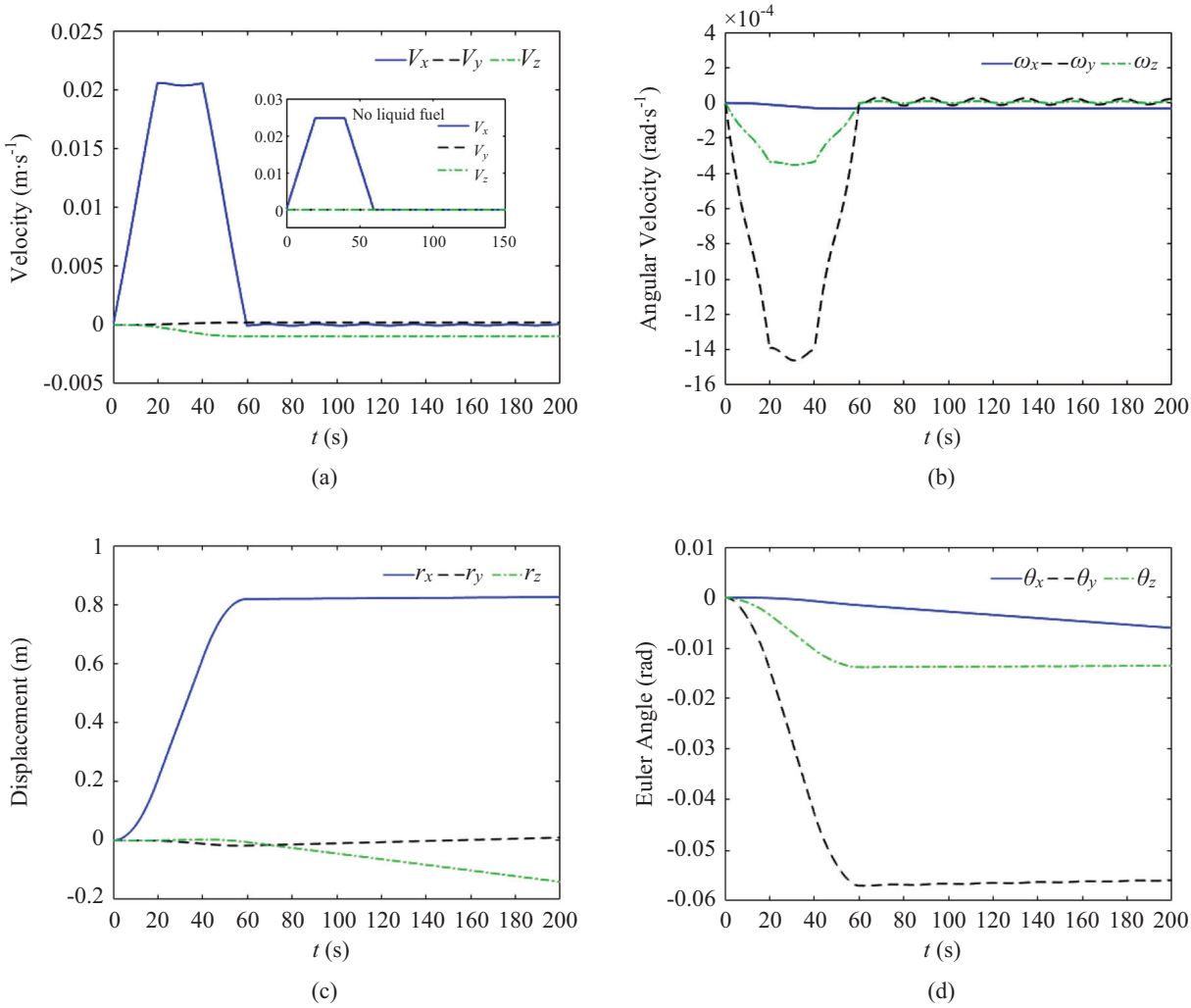


Fig. 6 Response of the spacecraft (a) velocity, (b) angular velocity, (c) displacement, (d) Euler angle.

applied to the coupled spacecraft system. The thruster firing actuates in the zero-momentum step driver mode in the *Ox* direction of the frame *Oxyz*, which can be represented by

$$F_x = \begin{cases} 1\text{N} & t < 20\text{s}, \\ -1\text{N} & 40\text{s} < t < 60\text{s}. \\ 0 & \text{other} \end{cases}$$

The response of the zero-momentum step driver mode will be considered. The center of the spherical container is located on (0.1 m, –0.15 m, 0.1 m) in the body frame *Oxyz*. Damping effect of sloshing liquid in the container has a non-negligible influence on the overall dynamics of the rigid-liquid coupled spacecraft, which should be considered in the dynamical analysis of the spacecraft system. The modal damping of the sloshing liquid is 0.01 [16]. The numerical simulation results are presented in Figs. 6-7. The following conclusions can be drawn from the numerical results: 1. Propellant sloshing has a non-negligible influence on the spacecraft attitude and position dynamic. Spacecraft unfavorable translation and rotation appeared after thruster turning off as showed in Fig. 6, which is due to liquid sloshing in the tank. The spacecraft system will be stationary with the same step driver mode if the liquid sloshing effect is neglected as showed in the top right corner of Fig. 6(a). 2. The value of the sloshing forces and sloshing moments are discontinuous when the thruster firing or turning off (Fig. 7(a) and (b)). The response of the sloshing parameters will be changed under the different driver mode form of the spacecraft, which reflected the coupling effects of the spacecraft to the propellant in the tank. 3. Although zero-momentum step driver mode is only in the *Ox* direction, sloshing forces will be appeared in other directions. These indicated the complexity of the liquid sloshing. 4. The primary planar or nonplanar primary sloshing modal is the dominant liquid sloshing mode. 5. There is a huge difference of the dynamic responses of the coupled spacecraft system between the thruster firing and turning off. The amplitude of the sloshing parameters is larger when the thruster firing.

https://doi.org/10.1017/jmech.2018.15 Published online by Cambridge University Press

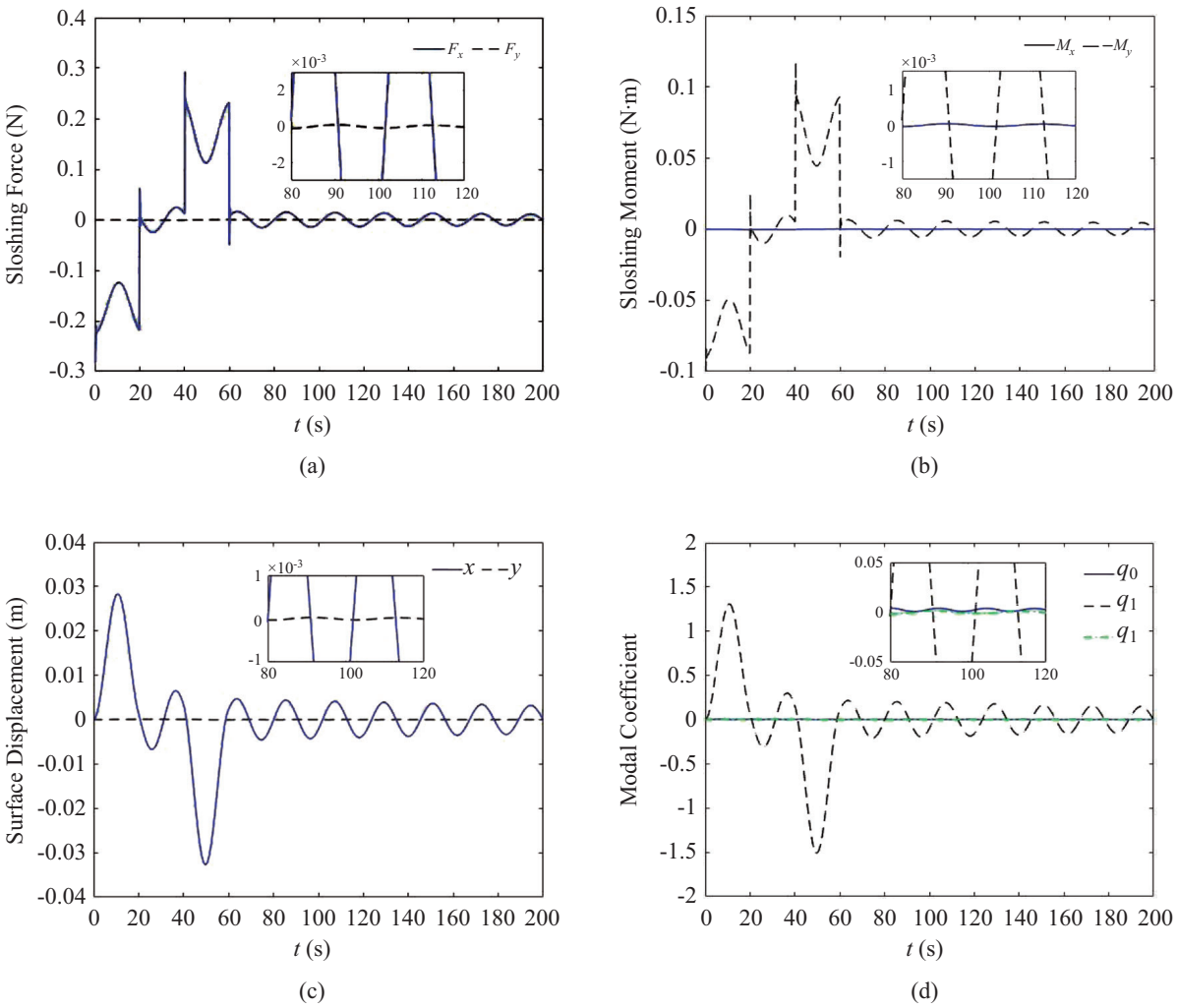


Fig. 7 Response of the sloshing parameters (a) sloshing force, (b) sloshing moment, (c) sloshing wave height at the tank wall, (d) modal coefficient.

4. CONCLUSIONS

In this paper, the rigid-coupled dynamical behaviors of the spacecraft with the arbitrary axisymmetric tank were considered. The governing equations of sloshing modal coordinates were developed through the Galerkin method. Lagrange's equations in term of general quasi-coordinates were used to construct the state equations of the coupled motion of main rigid platform of the spacecraft. The response of the coupled rigid-liquid was studied under the harmonic excitation and the zero-momentum step driver mode via numerical simulations. Research results showed that the rigid-liquid coupled spacecraft system exhibits complex dynamical behavior such as quasi-periodical motion, beat vibration, resonance with the variation of the external excitation frequency. The rigid-liquid coupled spacecraft system appeared some meaningful phenomena when thruster firing actuates in the zero-momentum step mode. Propellant sloshing has a non-negligible influence on the spacecraft attitude and position dynamics, and the motions of the spacecraft also exerted influence on the propellant sloshing in the tank. Although zero momentum step driver mode only acts in one direction, sloshing forces will be arising in other directions. The amplitude of the sloshing responses will be larger when the thruster begins to fire or turn off. The model developed in this paper can be utilized to arbitrary axisymmetric tank such as spherical, prolate spherical, oblate spherical, and Cassini tank, which have a reference value to the overall design of the spacecraft system.

ACKNOWLEDGEMENTS

The authors sincerely acknowledge the financial support of the National Natural Science Foundation of China (NNSFC) through Grants No. 11472041, 11772049 and 11532002.

https://doi.org/10.1017/jmech.2018.15 Published online by Cambridge University Press

APPENDICES

The detailed descriptions of the symbols in Eq. (8).

$$R_{W\theta}=\frac{\partial R_W}{\partial\theta},\quad R_{M\theta}=\frac{\partial R_M}{\partial\theta},\quad \zeta_\theta=\frac{\partial\zeta}{\partial\theta},\quad \zeta_{\theta\theta}=\frac{\partial^2\zeta}{\partial\theta^2},\quad \zeta_{\varphi\varphi}=\frac{\partial^2\zeta}{\partial\varphi^2},$$

$$S_{0M}=R_M^{-1}(R_M^2+R_{M\theta}^2)^{-3/2}[R_M(2R_M^2+3R_{M\theta}^2-R_MR_{M\theta\theta})-\cot\theta R_{M\theta}(R_M^2+R_{M\theta}^2)]$$

$$S_{1M}=R_M^{-2}(R_M^2+R_{M\theta}^2)^{-5/2}[R_M(2R_M^4+5R_M^2R_{M\theta}^2+6R_{M\theta}^4-3R_MR_{M\theta}^2R_{M\theta\theta})-\cot\theta R_{M\theta}^3(R_M^2+R_{M\theta}^2)]$$

$$S_{2M}=R_M^{-1}(R_M^2+R_{M\theta}^2)^{-5/2}[3R_MR_{M\theta}(R_{M\theta}R_{M\theta\theta}-R_{M\theta}^2)-\cot\theta R_M^2(R_M^2+R_{M\theta}^2)]$$

$$S_{3M}=-R_M(R_M^2+R_{M\theta}^2)^{-3/2},$$

$$S_{4M}=-\sin^{-2}\theta R_M^{-1}(R_M^2+R_{M\theta}^2)^{-1/2}.$$

The detailed descriptions of the symbols in Eq. (12)，where m = 0, 1, 2, …

$$M_m=-\varepsilon\rho_f\int_0^{\bar\theta}\sum_{l=1}^{\infty}\left[a_{ml}\left(R_W/l_a\right)^{-(1+\alpha_{ml})}+b_{ml}\left(R_W/l_b\right)^{\alpha_{ml}}\right]\Theta_{ml}\left\{\sum_{k=1}^{\infty}\left[-(1+\alpha_{mk})a_{mk}\left(R_W/l_a\right)^{-(2+\alpha_{mk})}/l_a\right.\right.$$

$$\left.+b_{mk}\alpha_{mk}\left(R_W/l_b\right)^{\alpha_{mk}-1}/l_b\right]\Theta_{mk}-\frac{R_{W\theta}}{R_W^2}\sum_{k=1}^{\infty}\left[a_{mk}\left(R_W/l_a\right)^{-(1+\alpha_{mk})}+b_{mk}\left(R_W/l_b\right)^{\alpha_{mk}}\right]\Theta'_{mk}\left.\right\}R_W^2\sin\theta\mathrm{d}\theta$$

$$-\varepsilon\rho_f\int_0^{\bar\theta}a_{ml}\left(R_M/l_a\right)^{-(1+\alpha_{ml})}+b_{ml}\left(R_M/l_b\right)^{\alpha_{ml}}\Theta_{ml}\left\{\sum_{k=1}^{\infty}c_{mk}\Theta_{mk}-\sum_{k=1}^{\infty}\left[-(1+\alpha_{mk})a_{mk}\left(R_M/l_a\right)^{-(2+\alpha_{mk})}/l_a\right.\right.$$

$$\left.+b_{mk}\alpha_{mk}\left(R_M/l_b\right)^{\alpha_{mk}-1}/l_b\right]\Theta_{mk}+\frac{R_{M\theta}}{R_M^2}\sum_{k=1}^{\infty}\left[a_{mk}\left(R_M/l_a\right)^{-(1+\alpha_{mk})}+b_{mk}\left(R_M/l_b\right)^{\alpha_{mk}}\right]\Theta'_{mk}\left.\right\}R_M^2\sin\theta\mathrm{d}\theta$$

$$+\varepsilon\rho_f\int_0^{\bar\theta}\sum_{k=1}^{\infty}\left[a_{mk}\left(R_M/l_a\right)^{-(1+\alpha_{mk})}+b_{mk}\left(R_M/l_b\right)^{\alpha_{mk}}\right]\Theta_{mk}\sum_{l=1}^{\infty}c_{ml}\Theta_{ml}R_M^2\sin\theta\mathrm{d}\theta$$

$$K_m=\int_0^{\bar\theta}\sum_{k=1}^{\infty}c_{mk}\left\{[-\rho_f(g+\dot v_z+\dot\omega_xy_i-\dot\omega_yx_i)\cos\theta-\sigma S_{1M}+m^2\sigma S_{4M}]\Theta_{mk}\right.$$

$$\left.-\sigma S_{2M}\Theta'_{mk}-\sigma S_{3M}\Theta''_{mk}\right\}\sum_{l=1}^{\infty}c_{ml}\Theta_{ml}R_M^2\sin\theta\mathrm{d}\theta$$

$$\beta_0=-\int_0^{\bar\theta}\{\varepsilon2\kappa_0\sigma+\rho_fg(R_M(0)-R_M(\theta)\cos\theta)+\varepsilon\rho_f(h_i-\varepsilon R_M\cos\theta)(\dot v_z+\dot\omega_xy_i-\dot\omega_yx_i)\}\sum_{l=1}^{\infty}c_{0l}\Theta_{0l}R_M^2\sin\theta\mathrm{d}\theta,$$

$$\beta_1=-\varepsilon\rho_f(\dot v_x+\dot\omega_yz_i-\dot\omega_zy_i)\int_0^{\bar\theta}\sum_{l=1}^{\infty}c_{1l}\Theta_{1l}R_M^3\sin^2\theta\mathrm{d}\theta,$$

$$\beta_2=-\varepsilon\rho_f(\dot v_y+\dot\omega_zx_i-\dot\omega_xz_i)\int_0^{\bar\theta}\sum_{l=1}^{\infty}c_{1l}\Theta_{1l}R_M^3\sin^2\theta\mathrm{d}\theta.$$

The detailed descriptions of sloshing forces and sloshing moments.

$$F_{xi}=-\pi\rho_f\varepsilon\int_0^{\bar\theta}\left\{\sum_{k=1}^{\infty}\left[a_{1k}\left(R_W/l_a\right)^{-(1+\alpha_{1k})}+b_{1k}\left(R_W/l_b\right)^{\alpha_{1k}}\right]\Theta_{1k}\ddot q_1+(\dot v_x+\dot\omega_yz_i-\dot\omega_zy_i)\sin\theta R_W\right\}$$

$$\times(R_W\sin\theta-R_{W\theta}\cos\theta)R_W\sin\theta\mathrm{d}\theta+\varepsilon\pi\{2\kappa_0\sigma+\varepsilon\rho_fg[R_M(0)-R_M(\bar\theta)\cos\bar\theta]\}$$

$$\times\sum_{k=1}^{\infty}c_{1k}\Theta_{1k}(\bar\theta)q_1\cos\bar\theta R_M\sin\bar\theta+\frac{\sigma\pi}{[R_M^2(\bar\theta)+R_{M\theta}^2(\bar\theta)]^{3/2}}\sum_{k=1}^{\infty}c_{1k}\Theta_{1k}(\bar\theta)q_1\{-R_{M\theta}^3(\bar\theta)\sin^2\bar\theta$$

$$-R_M(\bar\theta)[R_M^2(\bar\theta)+2R_{M\theta}^2(\bar\theta)]\sin\bar\theta\cos\bar\theta+[R_M^2(\bar\theta)+R_{M\theta}^2(\bar\theta)]R_{M\theta}(\bar\theta)\}$$

https://doi.org/10.1017/jmech.2018.15 Published online by Cambridge University Press

$$F_{yi}=-\pi\rho_f\varepsilon\int_0^{\bar\theta}\left\{\sum_{k=1}^{\infty}[a_{1k}\left(R_W/l_a\right)^{-(1+\alpha_{1k})}+b_{1k}\left(R_W/l_b\right)^{\alpha_{1k}}]\Theta_{1k}\ddot p_1+(\dot v_y+\dot\omega_z x_i-\dot\omega_x z_i)\sin\theta R_W\right\}$$

$$\times(R_W\sin\theta-R_{W\theta}\cos\theta)R_W\sin\theta\mathrm{d}\theta+\varepsilon\pi\{2\kappa_0\sigma+\varepsilon\rho_f g[R_M(0)-R_M(\bar\theta)\cos\bar\theta]\}$$

$$\times\sum_{k=1}^{\infty}c_{1k}\Theta_{1k}(\bar\theta)p_1\cos\bar\theta R_M\sin\bar\theta+\frac{\sigma\pi}{(R_M^2(\bar\theta)+R_{M\theta}^2(\bar\theta))^{3/2}}\sum_{k=1}^{\infty}c_{1k}\Theta_{1k}(\bar\theta)p_1\{-R_{M\theta}^3(\bar\theta)\sin^2\bar\theta$$

$$-R_M(\bar\theta)[R_M^2(\bar\theta)+2R_{M\theta}^2(\bar\theta)]\sin\bar\theta\cos\bar\theta+[R_M^2(\bar\theta)+R_{M\theta}^2(\bar\theta)]R_{M\theta}(\bar\theta)\}$$

$$F_{zi}=-2\pi\rho_f\int_0^{\tilde\theta}\left\{\sum_{k=1}^{\infty}\left[a_{0k}\left(R_W/l_a\right)^{-(1+\alpha_{0k})}+b_{0k}\left(R_W/l_b\right)^{\alpha_{0k}}\right]\Theta_{0k}(\theta)\ddot q_0+(\dot v_z+\dot\omega_x y_i-\dot\omega_y x_i)(h_i-\varepsilon R_W\cos\theta_{pi})\right\}$$

$$(-R_W\cos\theta+R_{W\theta}\sin\theta)R_W\sin\theta\mathrm{d}\theta+2\pi\{2\kappa_0\sigma+\varepsilon\rho_f g[R_M(0)-R_M(\bar\theta)\cos\bar\theta]\}$$

$$\sum_{k=1}^{\infty}c_{0k}\Theta_{0k}(\bar\theta)q_0R_M\sin^2\bar\theta+\frac{2\varepsilon\sigma\pi}{[R_M^2(\bar\theta)+R_{M\theta}^2(\bar\theta)]^{3/2}}\times\sum_{k=1}^{\infty}c_{0k}\Theta_{0k}(\bar\theta)q_0\{R_{M\theta}^3(\bar\theta)\sin\bar\theta\cos\bar\theta$$

$$-R_M(\bar\theta)[R_M^2(\bar\theta)+2R_{M\theta}^2(\bar\theta)]\sin^2\bar\theta\}$$

$$M_{xi}=-\rho_f\pi\int_0^{\bar\theta}\left\{\sum_{k=1}^{\infty}a_{1k}\left(R_W/l_a\right)^{-(1+\alpha_{1k})}+b_{1k}\left(R_W/l_b\right)^{\alpha_{1k}}\Theta_{1k}\ddot p_1+(\dot v_y+\dot\omega_z x_i-\dot\omega_x z_i)\sin\theta R_W\right\}$$

$$\times[-(R_W\sin\theta-R_{W\theta}\cos\theta)h_i-\varepsilon R_{W\theta}R_W]R_W\sin\theta\mathrm{d}\theta$$

$$+\pi\varepsilon\{2\kappa_0\sigma+\varepsilon\rho_f g[R_M(0)-R_M(\bar\theta)\cos\bar\theta]\}\sum_{k=1}^{\infty}c_{1k}\Theta_{1k}(\bar\theta)p_1[\varepsilon R_W(\bar\theta)-h_i\cos\theta]R_M(\bar\theta)\sin\bar\theta$$

$$+\frac{\sigma\pi}{(R_M^2(\bar\theta)+R_{M\theta}^2(\bar\theta))^{3/2}}\sum_{k=1}^{\infty}c_{1k}\Theta_{1k}(\bar\theta)p_1\{-h\sin^2\bar\theta R_{M\theta}^3(\bar\theta)-R_M(\bar\theta)\sin\bar\theta[h\cos\bar\theta-\varepsilon R_M(\bar\theta)]$$

$$\times[R_M(\bar\theta)+2R_{M\theta}^2(\bar\theta)]+R_{M\theta}(\bar\theta)[h-\varepsilon R_M(\bar\theta)\cos\bar\theta][R_M^2(\bar\theta)+R_{M\theta}^2(\bar\theta)]\}$$

$$M_{yi}=-\rho_f\pi\int_0^{\bar\theta}\left\{\sum_{k=1}^{\infty}a_{1k}\left(R_W/l_a\right)^{-(1+\alpha_{1k})}+b_{1k}\left(R_W/l_b\right)^{\alpha_{1k}}\Theta_{1k}\ddot q_1+(\dot v_x+\dot\omega_y z_i-\dot\omega_z y_i)\sin\theta R_W\right\}$$

$$\times[\bar h_i(R_W\sin\theta-R_{W\theta}\cos\theta)+\varepsilon R_W R_{W\theta}]R_W\sin\theta\mathrm{d}\theta$$

$$+\pi\varepsilon\{2\kappa_0\sigma+\varepsilon\rho_f g[R_M(0)-R_M(\bar\theta)\cos\bar\theta]\}\sum_{k=1}^{\infty}c_{1k}\Theta_{1k}(\bar\theta)q_1[h_i\cos\theta-\varepsilon R_W(\bar\theta)]R_M(\bar\theta)\sin\bar\theta$$

$$+\frac{\sigma\pi}{(R_M^2(\bar\theta)+R_{M\theta}^2(\bar\theta))^{3/2}}\sum_{k=1}^{\infty}c_{1k}\Theta_{1k}(\bar\theta)q_1\{-h\sin^2\bar\theta R_{M\theta}^3(\bar\theta)-R_M(\bar\theta)\sin\bar\theta[h\cos\theta$$

$$-\varepsilon R_M(\bar\theta)][R_M(\bar\theta)+2R_{M\theta}^2(\bar\theta)]+R_{M\theta}(\bar\theta)[h-\varepsilon R_M(\bar\theta)\cos\bar\theta][R_M^2(\bar\theta)+R_{M\theta}^2(\bar\theta)]\}$$

$$M_{zi}=0$$

REFERENCES

1. Dodge, F. T., The New "Dynamic Behavior of Liquids in Moving Containers", NASA SP-106 (2000).
2. Deng, M. L. and Yue, B. Z., "Attitude Dynamics and Control of Liquid Filled Spacecraft with Large Amplitude Fuel Slosh," *Journal of Mechanics*, **33**, pp. 125-136 (2017).
3. Hung, R. J., Long, Y. T. and Zu, G. J., "Coupling of Gravity-Gradient-Dominated Acceleration-Induced Slosh Reaction Torques with Spacecraft Orbital Dynamics," *Control Engineering Practice*, **4**, pp. 939-949 (1996).
4. Hung, R. J., Long, Y. T. and Chi, Y. M., "Slosh Dynamics Coupled with Spacecraft Attitude Dynamics. I - Formulation and Theory," *Journal of Spacecraft and Rockets*, **33**, pp. 575-581 (1996).
5. Hastings, L. J. and Rutherford, R. I., "Low Gravity Liquid-Vapor Interface Shapes in Axisymmetric Containers and a Computer Solution," NASA TM X-53790 (1968)

https://doi.org/10.1017/jmech.2018.15 Published online by Cambridge University Press

6. Bauer, H. F. and Eidel, W., "Free and Forced Oscillations of a Frictionless Liquid in a Long Rectangular Tank with Structural Obstructions at the Free Liquid Surface," *Archive of Applied Mechanics*, **70**, pp. 550-560 (2000).
7. Bauer, H. F. and Eidel, W., "Hydroelastic Vibrations in a Two-Dimensional Rectangular Container Filled with Frictionless Liquid and a Partly Elastically Covered Free Surface," *Journal of Fluids and Structures*, **19**, pp. 209-220 (2004).
8. Yue, B. Z., Wu, W. J. and Yan, Y. L., "Modeling and Coupling Dynamics of the Spacecraft with Multiple Propellant Tanks," *AIAA Journal*, **54**, pp. 3608-3618 (2016).
9. Peterson, L. D., Crawley, E. F. and Hansman, R., "Nonlinear Fluid Slosh Coupled to the Dynamics of a Spacecraft," *AIAA Journal*, **27**, pp. 1230-1240 (1989).
10. Sabri, F. and Lakis, A. A., "Effects of Sloshing on Flutter Prediction of Liquid-Filled Circular Cylindrical Shell," *Journal of Aircraft*, **48**, pp. 1829-1839 (2011).
11. He, Y. J., Ma, X. R., Wang, P. P. and Wang, B. L., "Low-Gravity Liquid Nonlinear Sloshing Analysis in a Tank Under Pitching Excitation," *Journal of Sound and Vibration*, **299**, pp. 164-177 (2007).
12. McIver, P., "Sloshing Frequencies for Cylindrical and Spherical Containers Filled to an Arbitrary Depth," *Journal of Fluid Mechanics*, **201**, pp. 243-257 (1989).
13. Utsumi, M., "Low-Gravity Propellant Slosh Analysis Using Spherical Coordinates," *Journal of Fluids and Structures*, **12**, pp. 57-83 (1998).
14. Utsumi, M., "Low-Gravity Sloshing in an Axisymmetrical Container Excited in the Axial Direction," *Journal of Applied Mechanics-Transactions of the ASME*, **67**, pp. 344-354 (2000).
15. Utsumi, M., "Low-Gravity Slosh Analysis for Cylindrical Tanks with Hemiellipsoidal Top and Bottom," *Journal of Spacecraft and Rockets*, **45**, pp. 813-821 (2008).
16. Yang, D. D. and Yue, B. Z., "Research on Sloshing in Axisymmetrcal Containers Under Low Gravity," *Journal of Astronautics*, **34**, pp. 917-925 (2013).
17. Utsumi, M., "Slosh Damping Caused by Friction Work Due to Contact Angle Hysteresis," *AIAA Journal*, **55**, pp. 265-273 (2016).
18. Lü, J., Wang, S. M. and Wang, T. S., "Coupling Dynamic Analysis of a Liquid-Filled Spherical Container Subject to Arbitrary Excitation," *Acta Mechanica Sinica*, **28**, pp. 1154-1162 (2012).
19. Faltinsen, O. M. and Timokha, A. N., "Analytically Approximate Natural Sloshing Modes for a Spherical Tank Shape," *Journal of Fluid Mechanics*, **703**, pp. 391-401 (2012).
20. Yue, B. Z. and Zhu, L. M., "Hybrid Control of Liquid-Filled Spacecraft Maneuvers by Dynamic Inversion and Input Shaping," *AIAA Journal*, **52**, pp. 618-626 (2014).
21. Kana, D. D., "Validated Spherical Pendulum Model for Rotary Liquid Slosh," *Journal of Spacecraft and Rockets*, **26**, pp. 188-195 (1989).
22. Ahmad, S., Yue, B. Z. and Shah, S. F., "Hamilton Structure and Stability Analysis for a Partially Filled Container," *Journal of Mechanics*, **29**, pp. 79-83 (2012).
23. Dodge, F. T., Green, S. T. and Cruse, M. W., "Analysis of Small-Amplitude Low Gravity Sloshing in Axisymmetric Tanks," *Microgravity - Science and Technology*, **4**, pp. 228-234 (1991).
24. Veldman, A. E. P., Gerrits, J., Luppes, R., Helder, J. A. and Vreeburg, J. P. B., "The Numerical Simulation of Liquid Sloshing on Board Spacecraft," *Journal of Computational Physics*, **224**, pp. 82-99 (2007).
25. Kulczycki, T., Kwaśnicki, M. and Siudeja, B., "The Shape of the Fundamental Sloshing Mode in Axisymmetric Containers," *Journal of Engineering Mathematics*, **99**, pp. 157-183 (2016).
26. Ibrahim, R. A., *Liquid Sloshing Dynamics Theory and Applications*, 2nd Edition, Cambridge University Press, Cambridge, pp. 294-329 (2005).
27. Yang, A. S., "Investigation of Liquid–Gas Interfacial Shapes in Reduced Gravitational Environments," *International Journal of Mechanical Sciences*, **50**, pp. 1304-1315 (2008).
28. Storey, J. M., Kirk, D. R., Gutierrez, H., Marsell, B. and Schallhorn, P. A. "Experimental, Numerical and Analytical Characterization of Slosh Dynamics Applied to In-Space Propellant Storage and Management," *51st AIAA/SAE/ASEE Joint Propulsion Conference*, Orlando, FL (2015).

(Manuscript received March 17, 2017,
accepted for publication February 26, 2018.)

https://doi.org/10.1017/jmech.2018.15 Published online by Cambridge University Press